Article

Structural Analysis of Hybrid Titania-Based Mesostructured Composites

Shannon W. Boettcher, Michael H. Bartl, Jerry G. Hu, and Galen D. Stucky

J. Am. Chem. Soc., **2005**, 127 (27), 9721-9730• DOI: 10.1021/ja050753r • Publication Date (Web): 16 June 2005

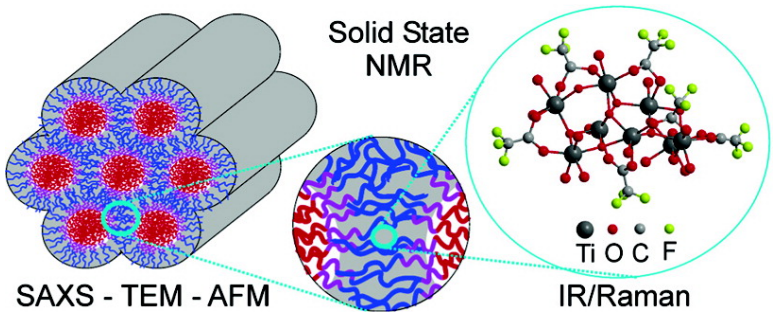

More About This Article

Additional resources and features associated with this article are available within the HTML version:

- Supporting Information
- Links to the 13 articles that cite this article, as of the time of this article download
- Access to high resolution figures
- Links to articles and content related to this article
- Copyright permission to reproduce figures and/or text from this article

View the Full Text HTML

J|A|C|S
ARTICLES
Published on Web 06/16/2005

Structural Analysis of Hybrid Titania-Based Mesostructured Composites

Shannon W. Boettcher, Michael H. Bartl, Jerry G. Hu, and Galen D. Stucky*

Contribution from the Department of Chemistry and Biochemistry, California NanoSystems Institute (CNSI), and the Materials Research Laboratory, University of California, Santa Barbara, California 93106

Received February 4, 2005; E-mail: stucky@chem.ucsb.edu

Abstract: High-optical-quality titania-based mesostructured films with cubic or 2D-hexagonal symmetry were fabricated by combining trifluoroacetate (TFA)-modified titanium precursors with amphiphilic triblock poly(ethylene oxide)−poly(propylene oxide)−poly(ethylene oxide) (PEO−PPO−PEO) copolymers. The distribution, dynamics, and local environments of the TFA-modified titania, PEO, and PPO components of the hybrid were investigated. IR/Raman spectroscopy, in situ small-angle X-ray scattering, and transmission electron microscopy studies indicate that TFA coordinates the titanium center and forms a stable complex that is subsequently organized by the block copolymer species into ordered mesostructures. Solid-state NMR $^{19}F\rightarrow{}^{1}H$ cross-polarization, $^{13}C\{^{1}H\}$ two-dimensional heteronuclear correlation, and ^{1}H relaxation techniques were used to determine that PEO is predominantly incorporated within the TFA-modified titania, and that PPO environments encompass both microphase separated regions and interfacial regions composed of mixed PPO and TFA-modified titania. NMR ^{19}F multiple-quantum spin counting measurements suggest that $-CF_3$ groups of the trifluoroacetate ligands do not form clusters but instead randomly distribute within the inorganic component of the hybrid.

Introduction

Hybrid materials—composites that combine attractive qualities of dissimilar materials—have received immense interest for a wide range of mechanical, electronic, magnetic, biological, and optical applications.[1] For use in optical applications, it is important that the length scale of the compositional inhomogeneities within a hybrid are on the order of nanometers—much less than typical photon wavelengths to avoid scattering.[2,3] In general, such "nanohybrid" or "nanocomposite" materials can be fabricated either by combining multiple presynthesized components into a final structure or by exploiting a one-pot synthesis, in which the composite structure is generated spontaneously during synthesis or processing. The latter is often preferable when multiple synthetic procedures are time-consuming or expensive.[4]

Ordered mesostructured materials fabricated from polymerizable silica species and organic structure-directing agents, such as amphiphilic block copolymers or charged surfactants, are important examples of self-assembling hybrids.[5−8] The ability to integrate specific functional molecules into distinct regions of the mesostructure is of particular interest.[9] For instance, when a laser dye is incorporated selectively into the organic domains of the mesostructure, silica-based hybrids perform a number of advanced optical applications, including optical switching and sensing, and low threshold waveguide microlasing.[3,10,11] However, optical devices fabricated from silica have a limited refractive index ($n = 1.43$) and must be supported by ultralow refractive index materials when efficient waveguiding is important.[11]

The next innovation in fabrication of ordered self-assembling optical hybrids required replacing the silica framework with a higher refractive index material, such as titania.[7,12−15] However, the chemistry of transition metal oxide precursors is more difficult to control;[6,16,17] not only must the hydrolysis/condensa-

(1) (a) Gomez-Romero, P.; Sanchez, C. *Functional Hybrid Materials*; Wiley: New York, 2004. (b) Kickelbick, G. *Prog. Polym. Sci.* **2003**, *28*, 83−114.
(2) (a) Beecroft, L. L.; Ober, C. K. *Chem. Mater.* **1997**, *9*, 1302−1317. (b) Prasad, P. N. *Curr. Opin. Solid State Mater. Sci.* **2004**, *8*, 11−19.
(3) Scott, B. J.; Wirnsberger, G.; Stucky, G. D. *Chem. Mater.* **2001**, *13*, 3140−3150.
(4) (a) Whitesides, G. M.; Grzybowski, B. *Science* **2002**, *295*, 2418−2421. (b) Alivisatos, A. P.; Barbara, P. F.; Castleman, A. W.; Chang, J.; Dixon, D. A.; Klein, M. L.; McLendon, G. L.; Miller, J. S.; Ratner, M. A.; Rossky, P. J.; Stupp, S. I.; Thompson, M. E. *Adv. Mater.* **1998**, *10*, 1297−1336. (c) Colfen, H.; Mann, S. *Angew. Chem., Int. Ed.* **2003**, *42*, 2350−2365.
(5) (a) Kresge, C. T.; Leonowicz, M. E.; Roth, W. J.; Vartuli, J. C.; Beck, J. S. *Nature* **1992**, *359*, 710−712. (b) Yanagisawa, T.; Shimizu, T.; Kuroda, K.; Kato, C. *B. Chem. Soc. Jpn.* **1990**, *63*, 988−992.
(6) Huo, Q. S.; Margolese, D. I.; Ciesla, U.; Feng, P. Y.; Gier, T. E.; Sieger, P.; Leon, R.; Petroff, P. M.; Schuth, F.; Stucky, G. D. *Nature* **1994**, *368*, 317−321.
(7) Alberius, P. C. A.; Frindell, K. L.; Hayward, R. C.; Kramer, E. J.; Stucky, G. D.; Chmelka, B. F. *Chem. Mater.* **2002**, *14*, 3284−3294.
(8) (a) Grosso, D.; Cagnol, F.; Soler-Illia, G. J. D. A.; Crepaldi, E. L.; Amenitsch, H.; Brunet-Bruneau, A.; Bourgeois, A.; Sanchez, C. *Adv. Funct. Mater.* **2004**, *14*, 309−322. (b) Brinker, C. J.; Lu, Y. F.; Sellinger, A.; Fan, H. Y. *Adv. Mater.* **1999**, *11*, 579−585.
(9) (a) Minoofar, P. N.; Hernandez, R.; Chia, S.; Dunn, B.; Zink, J. I.; Franville, A. C. *J. Am. Chem. Soc.* **2002**, *124*, 14388−14396. (b) Hernandez, R.; Franville, A. C.; Minoofar, P.; Dunn, B.; Zink, J. I. *J. Am. Chem. Soc.* **2001**, *123*, 1248−1249. (c) Frindell, K. L.; Bartl, M. H.; Popitsch, A.; Stucky, G. D. *Angew. Chem., Int. Ed.* **2002**, *41*, 959−962. (d) Bartl, M. H.; Scott, B. J.; Huang, H. C.; Wirnsberger, G.; Popitsch, A.; Chmelka, B. F.; Stucky, G. D. *Chem. Commun.* **2002**, *21*, 2474−2475.
(10) Wirnsberger, G.; Stucky, G. D. *Chem. Mater.* **2000**, *12*, 2525−2527.
(11) Yang, P. D.; Wirnsberger, G.; Huang, H. C.; Cordero, S. R.; McGehee, M. D.; Scott, B.; Deng, T.; Whitesides, G. M.; Chmelka, B. F.; Buratto, S. K.; Stucky, G. D. *Science* **2000**, *287*, 465−467.

tion reactions be finely tuned to match the kinetics of the self-organization but also must the material be easily patterned into optically transparent structures that are stable without heat treatment, which would destroy organic dyes. Recently, we have fabricated dye-doped hybrid waveguides with trifluoroacetate-modified titania frameworks and a high effective index of refraction ($n = 1.6-1.7$) that exhibit low threshold amplified spontaneous emission (ASE) type lasing when deposited directly onto glass substrates.[14] This material provides several advantages over previously reported synthetic routes that rely on inorganic acids for stabilization of the titania precursor. Crack-free thick films ($>10\ \mu$m) for optical waveguiding and lasing applications are easily fabricated using this new method, whereas thick films fabricated via inorganic-acid-based routes lack optical clarity.[7,13,15] Additionally, films fabricated via inorganic-acid-based routes require heat treatment to form a stable solid material that is incompatible with organic dye additives, whereas the modified titania hybrids are stable under ambient conditions for several months without heat treatment. Such titania-based nanocomposites are an important new class of easily processable high-refractive-index hybrid materials whose further development depends intimately on a detailed understanding of the material's structure over all relevant length scales and of the chemical interactions that dictate the assembly process.[18]

Herein, we report the synthesis and detailed characterization, from molecular to macroscopic length scales, of highly ordered, stable, titania-based hybrid optical materials fabricated from self-assembling block copolymers (P123 or F127) and trifluoroacetic acid (TFAA)-modified titania precursors, using advanced solid-state nuclear magnetic resonance (NMR) techniques combined with transmission electron microscopy (TEM), small-angle X-ray scattering (SAXS), atomic force microscopy (AFM), and IR/Raman spectroscopy. The resulting information, based upon interactions between each component of the hybrid material, allows for the creation of a structural model that encompasses molecular to macroscopic size regimes. In particular, we develop an understanding of the interfacial structure between dissimilar domains in the hybrid. This is especially important for nanostructured materials, where this "interphase" can be an appreciable fraction of the total solid.[19] To the best of our knowledge, this work includes the first NMR investigation of interfacial and molecular structures of ordered titania−surfactant "nanohybrids"—an expansive research area over the past several years.[7,13,15,20]

Experimental Section

Mesostructured Hybrid Film Preparation. Precursor solutions for mesostructured hybrids with hexagonal order were synthesized by adding 2.3 g of poly(ethylene oxide)$_{20}$−poly(propylene oxide)$_{70}$−poly(ethylene oxide)$_{20}$ nonionic surfactant (Pluronic P123, BASF) to 10 g of ethanol and stirring until the surfactant was fully dissolved. Separately, 3.9 mL of titanium (IV) ethoxide (TEOT 95% in ethanol, Aldrich) was reacted under heavy stirring with a mixture of 2.0 mL of trifluoroacetic acid (TFAA) (Merck) and 0.7 mL of hydrochloric acid (12.1 M). A precipitate initially formed, which redissolved upon rapid heating caused by exothermic reaction of H_2O and TFAA with TEOT (reaction of TEOT with pure TFAA is also highly exothermic). After 5 min, this solution was combined with the ethanolic surfactant solution and further stirred for at least 10 min. Precursors for the cubic films were prepared in a similar fashion, except poly(ethylene oxide)$_{106}$−poly(propylene oxide)$_{70}$−poly(ethylene oxide)$_{106}$ (Pluronic F127, BASF) was used as the surfactant due to its tendency to form a cubic mesophase.[21] Twelve grams of EtOH and 1 g of F127 were stirred under gentle heating until the surfactant completely dissolved. Separately, 3.9 mL of TEOT was reacted under heavy stirring with a mixture of 1.4 mL of TFAA and 1.3 mL of 12.1 M HCl. Solution viscosity was controlled by adjusting the amount of ethanol, thereby affecting the thickness of the final films. Films of variable thickness (100 nm to 10 μm) for either preparation were fabricated by dip- or spin-coating onto clean glass slides at various speeds. Films were placed directly in a 75% relative humidity chamber (controlled by saturated sodium chloride solution) at room temperature for a minimum of 24 h to maintain the fluidity of the surfactant mesophase and allow for a high degree of mesostructural order.[13] The films were then removed from the humidity chamber and allowed to fully dry. No heat treatment was necessary to stabilize the structure.

All $^{19}F\rightarrow{}^{1}H$ CPMAS and 2D $^{13}C\{^{1}H\}$ experiments were performed on deuterated samples fabricated from $CH_3CH_2O^2H$ (Aldrich), 35 wt % ^2HCl in ^2H_2O (Aldrich), TEOT (99.9% Alfa), and CF_3COO^2H (Alfa) in order to minimize cross-polarization to/from $-O^1H$ and ^1H_2O. In addition, the films were aged in a ^2H_2O humidity chamber, and NMR sample preparation was performed under N_2 purge to minimize ^1H_2O exchange with the ambient humidity. Deuterated samples had similar 1D X-ray diffraction patterns, and did not qualitatively differ in optical quality. 1-Fluoro-3,4,5-bromobenzene and silver trifluoroacetate (Aldrich) were used as received.

Characterization. Samples were prepared for NMR analysis by packing flakes of the material that had been scraped with a razor from multiple slides into a zirconia magic angle spinning (MAS) rotor. ^1H $T_1\rho$ relaxation, ^{13}C MAS, and $^{13}C\{^{1}H\}$ two-dimensional heteronuclear chemical shift correlation (HETCOR) experiments were performed at room temperature on a Bruker 500 MHz Avance spectrometer with a Bruker 4 mm MAS probe operating at 500.13 and 127.77 MHz for ^1H and ^{13}C, respectively. A spinning speed of 14 kHz was used, except in the case of the $^{13}C\{^{1}H\}$ HETCOR experiment, where 10 kHz spinning was employed. ^1H $T_1\rho$ relaxation rates were measured by directly observing ^1H signals. The pulse sequence employed consists of a 4.3 μs 90° pulse, followed by a spin locking field of $\nu_1 = 58.1$ kHz of variable duration. ^{13}C MAS experiments were performed employing two pulse phase modulated (TPPM) ^1H decoupling (66 kHz) with a recycle delay of 5 s and a ^{13}C 90° pulse length of 1.5 μs. $^{13}C\{^{1}H\}$ HETCOR experiments consisted of a 4.3 μs ^1H 90° pulse followed by a 2 ms ramp cross polarization (CP) contact time. TPPM ^1H decoupling (58 kHz) was applied during data acquisition; 512 $t1$ points and 1024

(12) (a) Vogel, R.; Meredith, P.; Kartini, I.; Harvey, M.; Riches, J. D.; Bishop, A.; Heckenberg, N.; Trau, M.; Rubinsztein-Dunlop, H. *ChemPhysChem* **2003**, *4*, 595−603. (b) Yang, P. D.; Zhao, D. Y.; Margolese, D. I.; Chmelka, B. F.; Stucky, G. D. *Nature* **1998**, *396*, 152−155. (c) Bartl, M. H.; Boettcher, S. W.; Frindell, K. L.; Stucky, G. D. *Acc. Chem. Res.* **2005**, *38*, 263−271.
(13) Crepaldi, E. L.; de Soler-Illia, G. J.; Grosso, D.; Cagnol, F.; Ribot, F.; Sanchez, C. *J. Am. Chem. Soc.* **2003**, *125*, 9770−9786.
(14) Bartl, M. H.; Boettcher, S. W.; Hu, E. L.; Stucky, G. D. *J. Am. Chem. Soc.* **2004**, *126*, 10826−10827.
(15) Yang, P.; Zhao, D.; Margolese, D. I.; Chmelka, B. F.; Stucky, G. D. *Chem. Mater.* **1999**, *11*, 2813−2826.
(16) (a) Brinker, C. J.; Scherer, G. W. *Sol−Gel Science, The Physics and Chemistry of Sol−Gel Processing*; Academic: London, 1990. (b) Antonelli, D. M.; Ying, J. Y. *Angew. Chem., Int. Ed.* **1996**, *35*, 426−430. (c) Antonelli, D. M.; Ying, J. Y. *Angew. Chem., Int. Ed.* **1995**, *34*, 2014−2017.
(17) Livage, J.; Henry, M.; Sanchez, C. *Prog. Solid State Chem.* **1988**, *18*, 259−341.
(18) Sanchez, C.; Soler-Illia, G. J. D. A.; Ribot, F.; Grosso, D. *C.R. Chim.* **2003**, 1131−1151.
(19) (a) Julian, B.; Gervais, C.; Cordoncillo, E.; Escribano, P.; Babonneau, F.; Sanchez, C. *Chem. Mater.* **2003**, *15*, 3026−3034. (b) Julian, B.; Gervais, C.; Rager, M. N.; Maquet, J.; Cordoncillo, E.; Escribano, P.; Babonneau, F.; Sanchez, C. *Chem. Mater.* **2004**, *16*, 521−529.
(20) (a) Yun, H. S.; Miyazawa, K.; Zhou, H. S.; Honma, I.; Kuwabara, M. *Adv. Mater.* **2001**, *13*, 1377−1380. (b) Yue, Y. H.; Gao, Z. *Chem. Commun.* **2000**, 1755−1756. (c) Antonelli, D. M. *Microporous Mesoporous Mater.* **1999**, *30*, 315−319. (d) Choi, S. Y.; Mamak, M.; Coombs, N.; Chopra, N.; Ozin, G. A. *Adv. Funct. Mater.* **2004**, *14*, 335−344.
(21) Holmqvist, P.; Alexandridis, P.; Lindman, B. *J. Phys. Chem. B* **1998**, *102*, 1149−1158.

*t*2 points were sampled, and a total of 4000 scans for each *t*1 point was collected.

^{19}F MAS,^{1}H→^{19}F CPMAS, and ^{19}F multiple-quantum (MQ) spin counting experiments were performed at room temperature on a Bruker 300 MHz Avance spectrometer operating at 300.09 and 282.34 MHz for ^{1}H and ^{19}F, respectively. ^{1}H→^{19}F CPMAS experiments were performed at a spinning speed of 10 kHz with a ^{1}H 90° pulse length of 6.6 μs using a ramp CP of variable duration. ^{19}F MQ NMR was performed under static conditions (4 mm rotor) using the 8-pulse even quantum propagator of Baum and Pines (90° pulse = Δ = 3.5 μs, Δ' = 10.5 μs, cycle time = 84 μs)[22,23] in a 2D phase incremented experiment[24,25] using 32 phase shifts and pulsed spin locking during data collection (512 ~ 57° *y* pulses interlaced between 40 μs sampling periods). Between 64 and 256 spectra were averaged for each phase shift. The resulting phase-incremented data were digitally repeated 512 times and Fourier transformed to obtain MQ stick spectra.[25] The MQ spectra were fit to Gaussian distributions whose standard deviation, σ, was associated with $(N/2)^{1/2}$, where N is the number of correlated spins. While these fits are not precise for small numbers of correlated spins, this is a convenient way to represent and compare the growth of the correlated spin system.[23]

In all cases, the chemical shifts of ^{1}H, ^{13}C, and ^{19}F were referenced to water, adamantane, and Teflon, respectively. Spectral fitting made use of the DMFIT program.[26]

One-dimensional-XRD was performed on a Scintag PAD X2 powder diffractometer, while 2D-SAXS and solution SAXS measurements were performed on a custom-built diffractometer, both using Cu Kα radiation. IR samples were prepared by dipping pressed KBr pellets into the precursor solution, while Raman samples were contained in glass capillaries. A Nicolet Magna 850 IR/Raman spectrometer was used to collect the spectra. TEM images were taken using a JEOL 2010 (for cubic films) or FEI T20 (for hexagonal films) electron microscope (200 keV). To prepare TEM samples, films were scraped from the substrate with a razor and dispersed in ethanol via quick grinding with mortar and pestle. One drop of this dispersion was deposited on a lacey-carbon-coated copper TEM grid and allowed to completely dry. Topographic measurements were made using a di-Dimension 3000 AFM.

Results and Discussion

To achieve a deep understanding of a hybrid material's structure, it is necessary to investigate a hierarchy of size scales with a diverse array of analysis techniques. First, we analyze molecular-level bonding interactions using IR and Raman spectroscopy. In the intermediate mesoscale size regime, SAXS and TEM are used to understand the assembly and structure of ordered hexagonal and cubic mesostructures. Since these materials find use as high-refractive-index optical waveguides,[14] "smooth" surface morphology over several length scales is demonstrated via optical and atomic force microscopy. The semi-local structural regime between the molecular and mesoscale (including molecular proximities and interfacial structure) is probed by a host of solid-state NMR experiments, including ^{19}F→^{1}H CPMAS, ^{13}C{^{1}H} HETCOR, ^{19}F MQ spin counting, and ^{1}H relaxation techniques.

Molecular Structure of Modified Titania. The chemical bonding mode between the carboxylic acid groups and the titanium centers was elucidated by IR and Raman spectroscopy,

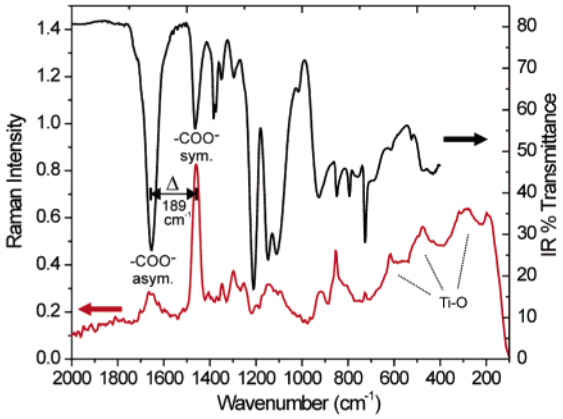

Figure 1. IR/Raman spectra of the hybrid material. TFA carboxylic acid stretches are indicative of bidentate bridging/chelation of the titanium center, and Ti−O stretches suggest rutile-like coordination in the amorphous inorganic.

Chart 1. Carboxylate Coordination Modes

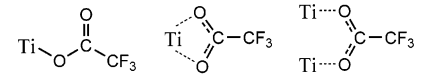

among the most well-developed analytical techniques for the characterization of organometallic complexes.[27] While acetic acid-modified titanium alkoxides have often been used for sol−gel processes,[28−30] fluorinated acids, such as TFAA, have seen little use.[31,32] The IR vibrations of the hybrid sample were assigned by comparison with IR spectra of the individual components as well as literature sources.[33] The observed IR/Raman spectra show TFA−Ti asymmetric (ν_{as} = 1653 cm^{-1}) and symmetric (ν_{sym} = 1464 cm^{-1}) carboxylate stretches (Figure 1). Low intensity stretches of free TFAA (1781 cm^{-1}) are apparent in freshly dipped films but completely disappear within 20 min of drying at room temperature. Identical vibrational transitions are observed in the ethanolic precursor solution.

The difference between carboxylate stretching frequencies, $\Delta = \nu_{as} - \nu_{sym}$, is useful in identifying the bonding mode of the carboxylate ligand (Chart 1).[27,34] Generally, monodentate complexes (A) exhibit Δ values much larger than those of the corresponding ionic structure (i.e., sodium trifluoroacetate). Bidentate chelating complexes (B) exhibit Δ values significantly smaller than the ionic values, and bridging complexes (C) have values less than, but close to, the ionic value. The observed Δ value for the hybrid material is 189 cm^{-1}, much smaller than that for isolated hydrogen bonded dimers[31] (345 cm^{-1}) or the

(22) Baum, J.; Pines, A. *J. Am. Chem. Soc.* **1986**, *108*, 7447−7454.
(23) Baum, J.; Munowitz, M.; Garroway, A. N.; Pines, A. *J. Chem. Phys.* **1985**, *83*, 2015−2025.
(24) Shykind, D. N.; Baum, J.; Liu, S. B.; Pines, A. *J. Magn. Reson.* **1988**, *76*, 149−154.
(25) Gleason, K. K. *Concepts Magn. Reson.* **1993**, *5*, 199−216.
(26) Massiot, D.; Fayon, F.; Capron, M.; King, I.; Le Calve, S.; Alonso, B.; Durand, J. O.; Bujoli, B.; Gan, Z. H.; Hoatson, G. *Magn. Reson. Chem.* **2002**, *40*, 70−76.
(27) Nakamoto, K. *Infrared and Raman Spectra of Inorganic and Coordination Compounds*; Wiley: New York, 1997.
(28) Livage, J.; Henry, M. A Predictive Model For Inorganic Polymerization. In *Ultrastructure Processing of Advanced Ceramics*; Ulrich, D. R., Mackenzie, J. D., Eds.; Wiley: New York, 1988; pp 183−195.
(29) Doeuff, S.; Henry, M.; Sanchez, C.; Livage, J. *J. Non-Cryst. Solids* **1987**, *89*, 206−216.
(30) Venz, P. A.; Kloprogge, J. T.; Frost, R. L. *Langmuir* **2000**, *16*, 4962−4968.
(31) Harrison, P. G.; Guest, A. *J. Chem. Soc., Faraday Trans.* **1991**, *87*, 1929−1934.
(32) (a) Yu, J. C.; Ho, W. K.; Yu, J. G.; Hark, S. K.; Iu, K. *Langmuir* **2003**, *19*, 3889−3896. (b) Niyogi, D. G.; Singh, S.; Saini, A.; Verma, R. D. *J. Fluor. Chem.* **1994**, *66*, 153−158.
(33) Socrates, G. *Infrared Characteristic Group Frequencies*; Wiley: New York, 1980.
(34) Deacon, G. B.; Phillips, R. J. *Coord. Chem. Rev.* **1980**, *33*, 227−250.

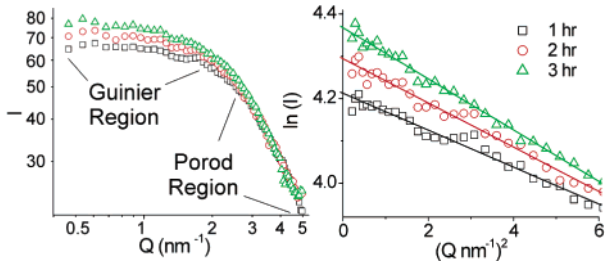

Figure 2. Left: Scattering data (log−log scale) showing typical scattering regimes for three 1 h time segments after solution preparation. Right: Linearized Porod region and fits used to determine R_g.

sodium salt[35] (~252 cm^{-1}). This establishes that TFA binds to the titanium center in a bidentate bridging or chelating fashion (C or B), both in solution and in the final hybrid. Because chelation (B) will strain the ~120° free carboxylate OCO bond angle, we suspect the TFA ligands bridge adjacent oxo/hydroxy-bridged titanium atoms (C) within the amorphous hybrid material.

The three broad, full-width-at-half-maximum (fwhm) 50−100 cm^{-1}, Raman intensities centered at ~600, ~475, and ~280 cm^{-1} (Figure 1) can be assigned to the Ti−O− network[30] and correspond approximately to the three vibrational transitions of the rutile phase of TiO_2 (612, 447, 232 cm^{-1}).[36] The sharp shoulders/peaks in the region were identified as structural deformations of the TFA ligand.[37] The Raman data suggest that the nearest neighbor environment around the central Ti ions consists of an octahedral "rutile-like" oxygen coordination, consistent with previous studies on acetic acid-modified titanium alkoxides.[28,30,38] The lack of long-range order between complexed titania species leads to an overall amorphous network.

Growth of Modified Titania Precursor and Block Copolymer Self-Assembly. The structure of the soluble TFA-modified titania species and their assembly can be further understood using SAXS techniques. The background-corrected scattering intensity as a function of scattering vector, $q = 4\pi \sin\theta/\lambda$, from the ethanolic precursor solution prepared without the structure-directing polymer (Figure 2, left) shows typical Porod and Guinier scattering regions.[39] The low q Guinier region, for which the approximation

$$I(q) = \Delta n_e \exp(-q^2 R_g^2/3) \quad (1)$$

holds, is particularly useful for analysis of particle sizes. R_g is defined as the radius of gyration[40] of the modified titanium precursors, and Δn_e is the electron density contrast between these precursors and the ethanolic solution. Plotting the low q data as the natural log of intensity versus q^2 yields linear plots whose slope gives R_g. As the sol solution aged, R_g grew from 3.6 ± 0.1 Å during the first hour to 4.0 ± 0.1 Å during the second hour and then to 4.3 ± 0.1 Å during the final hour of data collection. Our calculations show that these sizes are consistent with a molecular precursor consisting of ~4−5 Ti atoms connected by oxo/hydroxo linkages and bridging TFA molecules.[41] The precursor growth with time implies additional condensation from water generated by the esterification of TFAA by EtOH.[42]

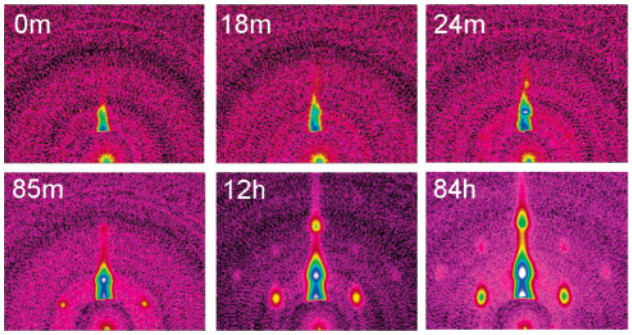

Figure 3. In situ 2D-SAXS patterns obtained following dip-coating. The time after dip-coating that data collection was started is given in the upper left of each pattern. The first two patterns were collected for 3 min apiece, the third 5 min, and the final three for 10 min.

The assembly of the inorganic precursor (identified from IR/SAXS measurements above) by the structure-directing block copolymer was followed using in situ 2D-SAXS. Such measurements have been used to understand both the kinetics of mesostructure formation and the phase pathways by which these processes take place.[13,43] Following dip-coating, the films were immediately placed in a humidity-controlled sample chamber (relative humidity = 75%) and data collection was started. The time-resolved 2D-SAXS results for the films with a hexagonal mesostructure (Figure 3) indicate that during the first 30 min after dip-coating, 1D periodicity perpendicular to the film surface develops, which may be due to a lamellar intermediate. This is consistent with an evaporation-induced self-assembly mechanism (EISA), where solvent evaporation after deposition concentrates the precursor solution and induces mesophase formation.[8] After the initial 30 min, the intensity of the hexagonal (11) peaks slowly grew and second-order peaks were observed after ~12 h. During the next week, the structure continued to organize, as evidenced by the growth in the peak intensities and appearance of higher-order peaks (Figure 4). The fact that the hybrid structure forms over an extended period of time suggests that TFA strongly inhibits extended condensation—consistent with the partial charge model (PCM),[28] which predicts a large negative partial charge on the electronegative TFA group and, therefore, a strong interaction with the positively charged metal center,[44] thereby making TFA a poor leaving group for substitution and condensation reactions.[17,28,45]

Analysis of the Final Mesostructure. Films of hybrid material deposited on glass slides were investigated in situ using SAXS. For these films, the 1D patterns are not sufficient to characterize the structure, due to the limited number of observed diffraction peaks (Figure 4, inset). In contrast, 2D-SAXS patterns yield detailed structural and texture information (Figure 4).

(35) Christe, K. O.; Naumann, D. *Spectrochim. Acta A* **1973**, *A29*, 2017−2024.
(36) Felske, A.; Plieth, W. J. *Electrochim. Acta* **1989**, *34*, 75−77.
(37) Berney, C. V. *J. Am. Chem. Soc.* **1973**, *95*, 708−716.
(38) Doeuff, S.; Henry, M.; Sanchez, C. *Mater. Res. Bull.* **1990**, *25*, 1519−1529.
(39) Porod, G. In *Small Angle X-ray Scattering*; Glatter, O., Kratky, O., Eds.; Academic Press: London, 1982; p 25.
(40) R_g can be thought of as the mean squared distance from the center of gravity where electrons play the role of mass.
(41) Simple models of cross-linked Ti−TFA−O networks consisting of 4−5 titanium atoms and 3−4 TFA groups yield calculated R_g values between 3.5 and 4.5 Å.
(42) Birnie, D. P. *J. Mater. Sci.* **2000**, *35*, 367−374.
(43) Doshi, D. A.; Gibaud, A.; Goletto, V.; Lu, M. C.; Gerung, H.; Ocko, B.; Han, S. M.; Brinker, C. J. *J. Am. Chem. Soc.* **2003**, *125*, 11646−11655.
(44) While the PCM might predict ion pair formation when large partial charges are formed, this is less favored in low dielectric environments, such as the ethanolic solution or solid.
(45) Sanchez, C.; Babonneau, F.; Doeuff, S.; Leaustic, A. Chemical Modifications of Titanium Alkoxide Precursors. In *Ultrastructure Processing of Advanced Ceramics*; Mackenzie, J. D., Ulrich, D. R., Eds.; Wiley: New York, 1988; pp 77−87.

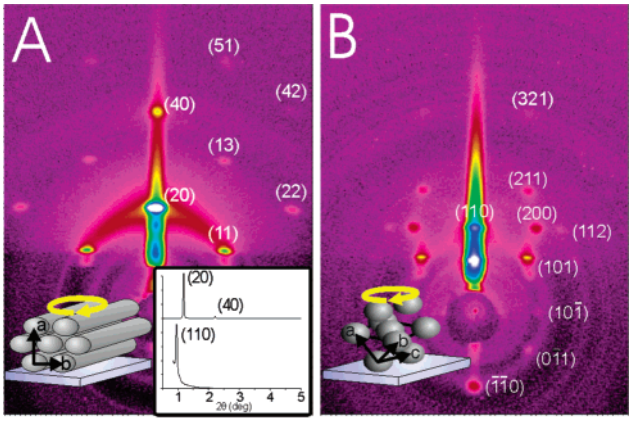

Figure 4. 2D-SAXS (log-scale of intensity) patterns of hybrid films collected in grazing incidence geometry. The patterns were fully assigned to distorted 2D-hexagonal (A) and distorted cubic (B) symmetries. The alignment of the real-space structure with respect to the substrate is shown. The yellow arrows indicate random orientation of the structure on the substrate plane. The 1D patterns are shown in the inset.

Patterns were collected at a grazing incidence angle of 0.4°, which is the cause of the observed reflected beam. The 1 mm thick SiO_2 substrate blocked the transmitted diffracted beams. However, for the cubic sample, weak peaks from transmitted intensity were observed, likely due to part of the film located at the very end of the substrate. The substrates were aligned such that the (110) or (20) diffraction spots correspond to planes parallel to the glass slide for cubic and hexagonal structures, respectively. All peaks in the cubic phase (Figure 4B) can be indexed to the distorted *Im*3*m* space group with lattice constants, $a = b = 15$ nm and $c = 17.5$ nm, similar to the previously reported cubic phase for F127.[13] The lattice distortion occurs due to contraction of the film perpendicular to the plane of the substrate during drying. The mesostructure is constructed of ordered domains for which the *c*-axis is aligned parallel with the plane of the substrate. Within the plane of the substrate, the *c*-vectors for individual domains are randomly oriented. Therefore, diffracted beams due to planes perpendicular to the film surface diffract for every orientation of the domain and are hence intense. All other planes diffract only for the specific domain orientations that bring the reciprocal lattice point onto the Ewald sphere and are, therefore, weaker in intensity.[46] Figure 4A shows the diffraction pattern from the distorted hexagonal structure corresponding to the plane group *C*2*m* with lattice constants $a = 16$ nm and $b = 11$ nm. Similar to the cubic structure, the *b*-vectors for different domains of the hexagonal phase are oriented randomly in the plane of the substrate—consistent with our observations from polarized light microscopy. Wide-angle scattering experiments showed no reflections, indicative of the amorphous nature of this material. The presence of higher-order reflections in both samples, (51) and (321), implies a high degree of mesostructural order in both cases.

While X-ray scattering techniques are sufficient to fully characterize the "average" mesostructure over a large area, TEM allows the direct visualization of the structure and reveals high degrees of order in both the hexagonal and cubic mesostructured hybrids (Figure 5). Figure 5A shows the cubic mesostructure along the [110] zone axis with distinct grain boundaries between

(46) Buerger, M. J. *Contemporary Crystallography*; McGraw-Hill: New York, 1970.

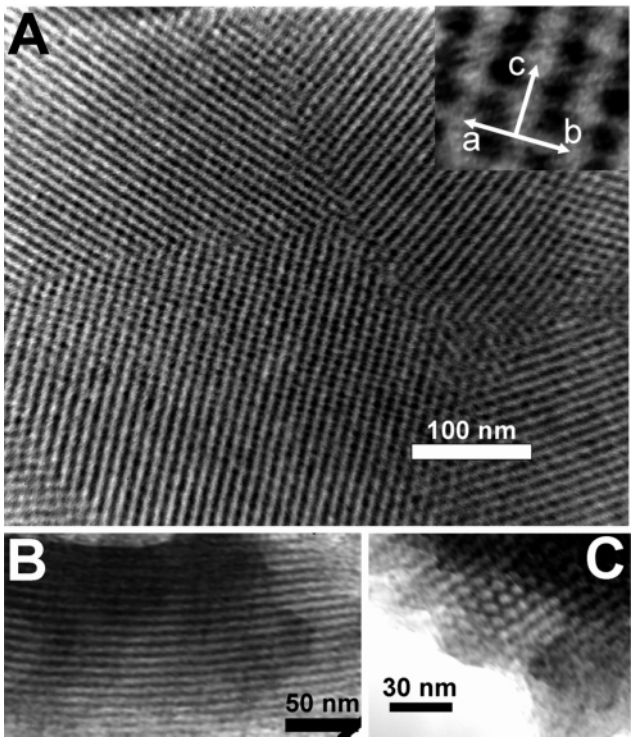

Figure 5. TEM micrographs of the as-synthesized hybrid material. (A) Micrograph of cubic hybrid material taken along the [110] zone axis exhibiting grain boundaries. Inset: Magnified region showing lattice vectors. (B) Hexagonal hybrid showing channel structure and (C) 2D packing.

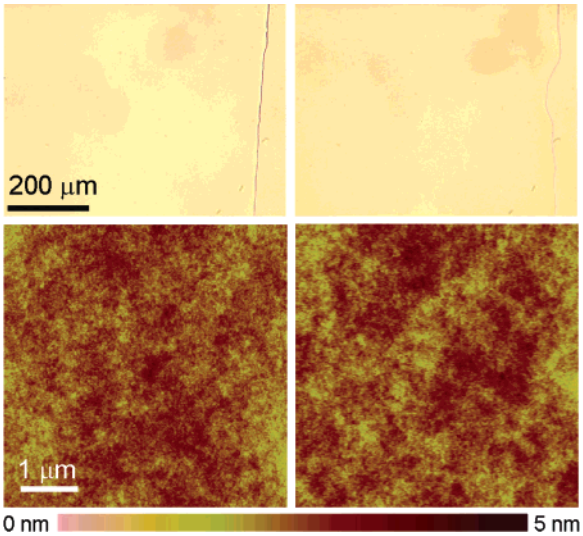

Figure 6. Optical micrographs (top) showing edge of film and AFM images (bottom) of hexagonal (left) and cubic (right) mesostructured hybrids.

domains with mismatched *c*-vectors. Figures 5B and 5C show the channel structure and the 2D-hexagonal close packing of the P123-templated film. Because these films were observed to shrink under the electron beam due to the high polymer content, lattice parameters were not extracted from TEM images.

Surface Characterization of the Hybrid Films. Visual inspection, optical microscopy, and AFM topographical imaging revealed smooth, crack-free films of the hybrid materials (Figure 6). Analysis of representative AFM height profiles from 25 μm^2 areas on the film surface yielded total height ranges of 6 and 3 nm and root-mean-squared (RMS) surface roughness values of 0.5 and 0.3 nm for cubic mesostructured films ~1.3 μm thick

and hexagonal mesostructured films ~3.6 μm thick, respectively. The observation that these materials are smooth over several orders of magnitude in length scale is extremely important for optical applications, including waveguiding and lasing.[14] While the surface parameters as a function of preparation method and film thickness were not studied in detail, in general, all films fabricated exhibited surface roughness parameters of the same order of magnitude.

Semi-Local Intermolecular and Interfacial Structure As Revealed by NMR. Modern solid-state NMR techniques, such as cross-polarization and two-dimensional (2D) experiments, can yield valuable information about molecular proximities and interfaces that is unavailable from TEM and SAXS experiments. These techniques have been used extensively in the characterization of silica/aluminosilicate-based hybrids (by exploiting the receptivity of ^{29}Si and ^{27}Al)[47,48] and organic polymer blends.[49−51] Due to the low abundance, low gyromagnetic ratio, moderately large quadrupole interaction, and the fact that there are two isotopes with different nuclear spin, ^{47,49}Ti NMR is experimentally challenging[52] and there have been no reports characterizing titania hybrids using this technique. ^{19}F, however, is an ideal nucleus for NMR, with 100% natural abundance, a large gyromagnetic ratio, and a nuclear spin of $^1/_2$.[53] Since a percentage of the titanium centers are coordinated by TFA ligands (vide supra), ^{19}F is an excellent probe of the local environment of the titania framework. In conjunction with ^{1}H and ^{13}C NMR experiments, we exploit ^{19}F NMR to examine, for the first time, the semi-local structure of titania-based hybrid materials. All NMR experiments were performed on the hybrid with hexagonal symmetry whose optical properties were investigated previously.[14]

TFA Content, Environment, and Distribution within the Hybrid Material. Solid-state ^{1}H-decoupled ^{13}C MAS experiments were used to quantify the relative amounts of TFA in the hybrid material (Figure 7). If we assume that the ratio of block copolymer to titanium precursor is unchanged from the precursor solution to the film, which is valid since neither species are volatile, then the Ti:TFA ratio can be calculated from the ^{13}C NMR signal integrations to be 1.7:1, meaning that only about 40% of the TFA added to the precursor solution remained within the composite material. TFA accounts for around 50 wt % of the "inorganic" network—a number corroborated by thermal gravimetric analysis data.

Since ^{19}F chemical shifts have a wide range (>1000 ppm) and are sensitive to chemical environment, direct ^{19}F MAS experiments were performed to assess chemical differences between TFA ligands. The ^{19}F MAS (35 kHz) experiment on the hybrid revealed a single sharp peak at −73.5 ppm with a

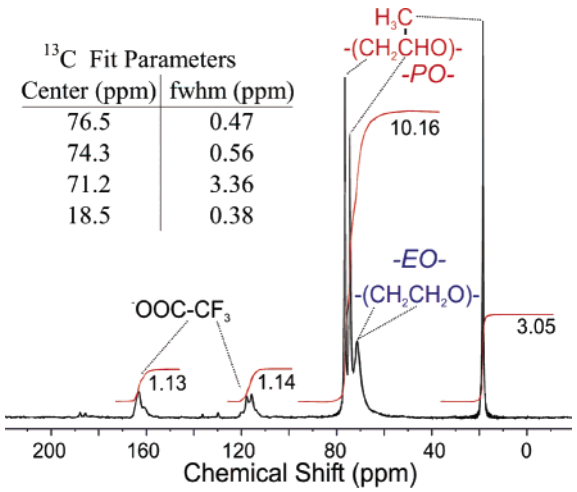

Figure 7. ^{13}C solid-state MAS spectrum (14 kHz) of hexagonally ordered hybrid material. *J*-coupling from the ^{19}F in the TFA is responsible for the splitting of the TFA carbon peaks. No signal from residual ethoxy groups is observed. Inset: fwhm from Lorenztian decomposition of polymer ^{13}C signals.

fwhm of 1.7 ppm (see Supporting Information). This indicates homogeneity of the chemical environment for the TFA ligands in the sample and suggests $-CF_3$ group rotational motion.

From the direct excitation experiments, we determined the relative TFA concentration and local environment, but we have little information about the spatial distribution of TFA within the solid. We hypothesized that either the TFA was homogeneously distributed or the TFA $-CF_3$ groups preferentially associate to form discrete clusters due to fluorocarbon philicity. MQ NMR using a pulse sequence designed to grow MQ coherent states between dipole-coupled nuclei was used to differentiate between these two cases.[23] Calculation of the number of correlated spins as a function of the length of the MQ preparation period reveals information about the spatial distribution of spins in a material[22] and has been used to study the distribution of fluorine-containing salts within polymer matrices.[54]

For the clustering case, the number of correlated spins as a function of preparation time should be steplike since the spins close to each other couple rapidly and intercluster coupling only occurs at longer preparation times. For evenly distributed spins, the cluster size is expected to grow continuously with preparation time. In our system, we observed rapid growth of the cluster size to ~3 correlated spins (coupling only within $-CF_3$ groups), followed by consistent growth of the system size with increasing preparation time (Figure 8, see also Supporting Information). For the preparation times examined, we did not observe the steplike behavior indicative of $-CF_3$ group clustering. To establish that we used preparation times adequate for correlation of spins within potential clusters, we performed the same experiment on a powdered silver trifluoroacetate sample, in which adjacent $-CF_3$ groups are in close spatial proximity. During identical preparation periods, the correlated spin system in silver trifluoroacetate grew much quicker than in the hybrid sample, reaching over 100 correlated spins in 504 μs. This verifies that if clusters of ^{19}F spins in close spatial proximity

(47) (a) Sindorf, D. W.; Maciel, G. E. *J. Am. Chem. Soc.* **1983**, *105*, 1487−1493. (b) Janicke, M. T.; Landry, C. C.; Christiansen, S. C.; Kumar, D.; Stucky, G. D.; Chmelka, B. F. *J. Am. Chem. Soc.* **1998**, *120*, 6940−6951. (c) De Paul, S. M.; Zwanziger, J. W.; Ulrich, R.; Wiesner, U.; Spiess, H. W. *J. Am. Chem. Soc.* **1999**, *121*, 5727−5736. (d) Templin, M.; Wiesner, U.; Spiess, H. W. *Adv. Mater.* **1997**, *9*, 814−817.
(48) Melosh, N. A.; Lipic, P.; Bates, F. S.; Wudl, F.; Stucky, G. D.; Fredrickson, G. H.; Chmelka, B. F. *Macromolecules* **1999**, *32*, 4332−4342.
(49) Johansson, A.; Tegenfeldt, J. *Macromolecules* **1992**, *25*, 4712−4715.
(50) Klein-Douwel, C. H.; Maas, W. E. J. R.; Veeman, W. S.; Werumeus-Buning, G. H.; Vankan, J. M. J. *Macromolecules* **1990**, *23*, 406−412.
(51) Schmidtrohr, K.; Clauss, J.; Spiess, H. W. *Macromolecules* **1992**, *25*, 3273−3277.
(52) Bastow, T. J.; Gibson, M. A.; Forwood, C. T. *Solid State Nucl. Magn.* **1998**, *12*, 201−209.
(53) Fry, R. A.; Tsomaia, N.; Pantano, C. G.; Mueller, K. T. *J. Am. Chem. Soc.* **2003**, *125*, 2378−2379.
(54) (a) Scruggs, B. E.; Gleason, K. K. *Macromolecules* **1992**, *25*, 1864−1869. (b) Limb, S. J.; Scruggs, B. E.; Gleason, K. K. *Macromolecules* **1993**, *26*, 3750−3757.

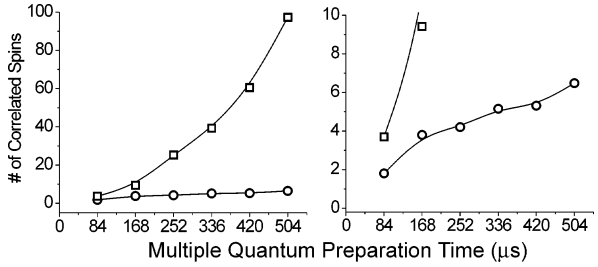

Figure 8. Growth of correlated spin system as a function of MQ preparation time for the hexagonal hybrid sample (○) and CF_3CO_2Ag powder (□). The left and right graphs are identical except for the *y*-axis scaling. The slow growth in the hybrid sample after an initial buildup to ~3 correlated spins indicates dispersed $-CF_3$ groups within the inorganic matrix and precludes cluster formation. Lines have been added to guide the eye.

were present in the hybrid sample, the preparation times investigated were adequate to observe the signature of these clusters (Figure 8). From this analysis, we concluded that $-CF_3$ group clusters are not present within the titania-based hybrid.

Analysis of Phase Segregation Based on Block Copolymer Mobility. The mobility of different copolymer blocks was used to gauge their respective degrees of interaction with the TFA−titania matrix. In general, sharp resonances in solid-state NMR spectra correspond to nuclei with large degrees of molecular motion because dipolar interactions and chemical shift anisotropy are effectively averaged out, whereas broad resonances indicate low mobility. Analysis of the decomposed ^{13}C spectrum (Figure 7) reveals that the signals corresponding to the poly(ethylene oxide) (PEO) carbons (70.17 ppm) of the block copolymer have a significantly larger fwhm than those corresponding to the poly(propylene oxide) (PPO) carbons. The lack of a sharp component to the PEO resonance is consistent with PEO-block incorporation within the rigid TFA−titania matrix.

The extent of microphase separation and mobilities of polymer segments can be better quantified by analysis of ^1H NMR relaxation rates. Such techniques have been used to investigate amorphous and crystalline domains in PEO[49] and PEO/PMMA blends[55] and to investigate microphase segregation in silica block copolymer monoliths.[48] Similar to semicrystalline polymer systems and silica composites, the PEO and PPO polymer segments may exhibit a distribution of mobilities depending on the structural environment of the polymer segment. This distribution of mobilities was analyzed by performing a series of experiments to extract the rotating-frame spin lattice relaxation time ($T_1\rho$) for each resolved peak in the ^1H spectra. This time constant describes the rate at which an excited ensemble of spins decays to thermal equilibrium with respect to the rotating reference frame under an applied magnetic field and is largely dependent on the dipolar coupling strength between protons. Molecular motion acts to average out the molecular interactions, and thus polymer segments occluded within the "rigid" inorganic matrix will have less mobility and thus shorter $T_1\rho$ times than those in microphase-segregated regions.[48]

^1H $T_1\rho$ values were obtained by collecting a series of 1D spectra in which a spin locking field of incremented duration was applied.[56] The normalized intensities of the PPO methyl peak and PEO/PPO $-CH_2-/-CH-$ backbone peak are plotted

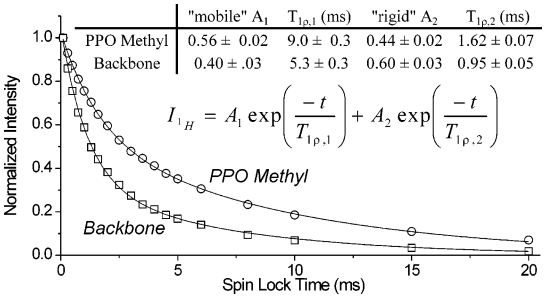

Figure 9. ^1H intensity as a function of spin lock times for the PPO methyl group (□) and the backbone (○) along with the biexponential fits (lines). The fitting equation and the best-fit parameters are included.

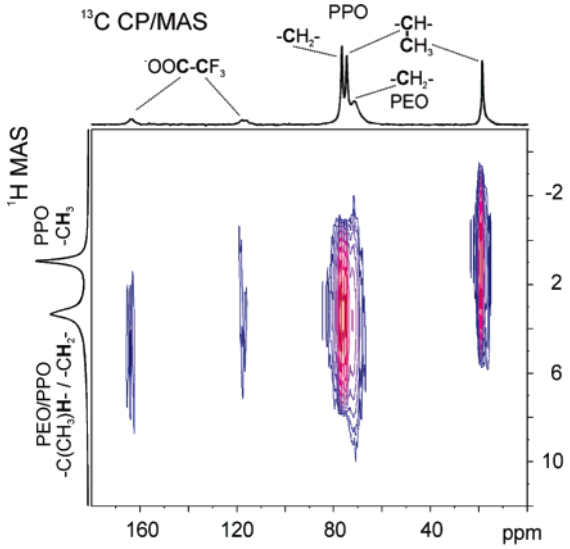

Figure 10. Two-dimensional HETCOR experiment shows spatial correlation between the TFA carbons and the PEO protons. Correlations between other pairs were not observed, likely due to the low signal-to-noise ratio in this experiment.

as a function of the spin locking pulse duration (Figure 9). The resulting data fit well to double exponential decays.[57]

Fitting the intensity data extracted from the PPO methyl group yielded two characteristic time constants (Figure 9) corresponding to "mobile" PPO segments (larger $T_1\rho$) and comparatively rigid PPO segments (smaller $T_1\rho$). While, in reality, there is a distribution of mobilities, these data suggest that the rigid portion of PPO is partially interacting with the inorganic phase—probably within an interfacial region between the PEO/inorganic and pure PPO (vide infra). This rigid PPO component is the cause of the broadened base of the PPO methyl peak in the $^1H \rightarrow ^{13}C$ CPMAS spectrum (Figure 10, top).

Although the backbone data also fit well to a biexponential decay, the analysis is complicated by the fact that the observed signal originates from both PPO and PEO segments. However, a stoichiometric calculation (EO/PO = 0.66 obtained from ^{13}C MAS) based on the ratio of mobile to rigid polymer for the PPO methyl peak reveals that nearly all of the mobile backbone intensity is due to the mobile segments on the PPO backbone—again, consistent with confinement of PEO within the TFA−titania.[48]

Interfacial Structure and Molecular Proximities as Assessed by 2D Correlation NMR and $^{19}F \rightarrow ^1H$ Cross-Polarization Dynamics. Because the ^{13}C signals of the TFA−Ti complexes are well separated from the ^{13}C polymer signals,

(55) Schantz, S. *Macromolecules* **1997**, *30*, 1419−1425.
(56) Komoroski, R. A. *High Resolution NMR Spectroscopy of Synthetic Polymers in Bulk*; VCH Publishers: New York, 1986.

HETCOR NMR spectroscopy, which has been used in the characterization of heterogeneous polymer blends,[51] is useful in understanding structure of these hybrid "inorganic polymer/organic block copolymer blends". This technique correlates specific ^{1}H and ^{13}C resonances in a 2D spectrum that allows identification of dipole−dipole-coupled nuclei. ^{1}H magnetization is created, which is transferred during the mixing time to ^{13}C nuclei within a specific proximity via heteronuclear dipole−dipole couplings.[58]

Figure 10 shows the 2D ^{13}C{^{1}H} HETCOR NMR spectrum of the hybrid material with separately acquired ^{1}H MAS and ^{13}C CPMAS spectra plotted along the respective axes. The ^{1}H MAS spectra consist of a peak at 1 ppm corresponding to the PPO methyl group and a broader peak at ∼3.4 ppm corresponding to PEO/PPO backbone protons.[59] The broader peak at ∼3.4 ppm was further decomposed into a narrow component centered at 3.4 ppm and a broad component centered at 3.9 ppm. The narrow component has a similar width as that of the PPO methyl group and was, therefore, assigned to the PPO backbone protons. The broad component was assigned to the PEO $-CH_2-$ backbone protons. In the 2D experiment, weak intensity correlation was observed between the TFA carbons and the protons on the PEO/PPO polymer backbone. The width and center of the TFA intensity correlation in the ^{1}H dimension correspond well to the broad ^{1}H peak assigned to the PEO. Furthermore, intensity correlation was not detected between the PPO methyl protons and the TFA carbons. These measurements suggest a spatial correlation between TFA and PEO that is much stronger than that between TFA and PPO. Since the overall sensitivity of this experiment is low and dilute correlations were not observable, this analysis is consistent with TFA−PPO contacts only within interfacial regions, whereas TFA−PEO contacts are present within the larger volume of the microphase-separated region.

Because both ^{1}H and ^{19}F are sensitive NMR nuclei, ^{19}F→^{1}H CPMAS can measure dipolar coupling over comparatively long distances (typically up to ∼1.4 nm), making it useful for determining local and intermediate structure of protons surrounding the TFA molecules in the composite.[60] In the ^{19}F→^{1}H CPMAS experiment, ^{19}F magnetization was created and transferred during the CP contact time (τ_{CP}) to nearby dipole-coupled protons. The experiment was repeated for a series of τ_{CP}'s, and the ^{1}H signal intensity for each resolved resonance was recorded. The rate at which the ^{1}H signal intensity increased for short τ_{CP}'s is indicative of strength of the ^{19}F−^{1}H dipolar coupling—which is strongly dependent on the shortest ^{19}F−^{1}H distances.

The ^{19}F→^{1}H CPMAS spectra were recorded as a function of CP contact time for the hybrid sample (Figure 11). Two narrow resonances at ∼1 and ∼3.5 ppm, which persist for long τ_{CP} (15 ms), were identified as PPO methyl and PPO backbone protons, respectively. The underlying broad resonance, which disappears at long τ_{CP}, results from protons on the PEO backbone. The

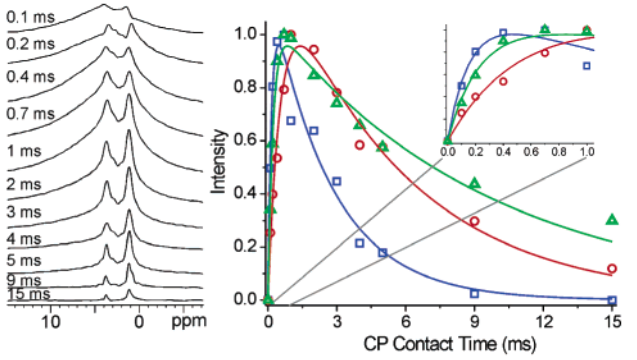

Figure 11. Left: ^{19}F→^{1}H CPMAS spectra as a function of CP contact time. Right: Integrated intensities for the PPO carbons (red circles), PEO carbons (blue squares), and $C_6Br_3H_2F$ (FBB) reference (green triangles) along with the double exponential fits.

Table 1. ^{19}F→^{1}H CPMAS Fit Parameters

	PEO	PPO	$C_6Br_3H_2F$
A	1.2 ± 0.1	1.4 ± 0.1	1.07 ± 0.04
T^*_{FH}	0.16 ± 0.03	0.54 ± 0.07	0.22 ± 0.02
$T^*_{1\rho}$	2.7 ± 0.3	5.6 ± 0.7	9.5 ± 1.0

increased width of the PEO signal is consistent with the ^{13}C NMR results that suggest incorporation into the bulk of the inorganic wall structure. CPMAS buildup curves were extracted by deconvoluting the spectra into a single broad PEO resonance and several narrow PPO resonances (Figure 11). We attribute the fact that the chemical shifts vary slightly as a function of mixing time to the distribution of polymer chemical environments. The integrated intensities of the signal assigned to the broad PEO segment and the sum of the integrated intensities of the multiple signals assigned to the PPO segment were plotted as a function of τ_{CP} (Figure 11). An identical experiment was performed on powdered 1-fluoro-3,4,5-bromobenzene (FBB) to allow for approximate comparison of ^{19}F−^{1}H distances.

The evolution of PEO, PPO, and FBB ^{1}H intensity was fit to a simple double exponential function of τ_{CP} (Table 1).

$$I(\tau_{CP}) = A\{\exp(-\tau_{CP}/T^*_{1\rho}) - \exp(-\tau_{CP}/T^*_{FH})\} \qquad (2)$$

where A is a fitting parameter for signal intensity. T^*_{FH} and $T^*_{1\rho}$ are *effective* parameters that characterize ^{1}H magnetization increases due to ^{19}F→^{1}H transfer and decreases due to rotating frame decay processes, respectively.[61] Because the distance between ^{19}F and ^{1}H spins is, to a first approximation, proportional to $(T^*_{FH})^{-6}$, analysis of T^*_{FH} for PPO, PEO, and FBB allows the comparison of the respective ^{19}F−^{1}H distances in each case.[50] The observation that $T^*_{FH,PEO}$ is similar to $T^*_{FH,FBB}$ (nearly within error) suggests that ^{19}F−^{1}H distances in both materials are comparable.[62]

Since in solid FBB we expect the ^{19}F−^{1}H distance to be mainly defined by the intramolecular pair distance, 2.7 Å, we estimate that the ^{19}F−^{1}H$_{PEO}$ distance is similar, ∼3 Å. Distances of this order imply that PEO is intimately mixed within the

(57) While such fits are not necessarily unique, they do provide an estimate of the relative amounts of mobile and rigid polymer segments.
(58) Duer, M. J. *Solid State NMR Spectroscopy*; Blackwell Science: Oxford, 2002.
(59) Flodstrom, K.; Wennerstrom, H.; Alfredsson, V. *Langmuir* **2004**, *20*, 680−688.
(60) Similar ^{19}F→^{13}C CPMAS experiments were completed. However, due to the low ^{19}F concentration, the low receptivity of ^{13}C, and the rotational motion of the $-CF_3$ group, which reduces dipolar couplings, only weak intensity from the covalently bonded TFA carbons was observed regardless of mixing time.
(61) Ando, S.; Harris, R. K.; Reinsberg, S. A. *J. Magn. Reson.* **1999**, *141*, 91−103.
(62) The direct comparison of coupling constants from different systems to assess distances is not precise because the proportionality constant depends on the molecular system of interest. However, the inverse sixth dependence of distance on the coupling constant ensures that errors due to these approximations will not greatly affect our conclusions.

TFA−titania framework. Although $T^*_{FH,PPO}$ is about three times $T^*_{FH,PEO}$, the corresponding $^{19}F-^{1}H$ distances only differ by a factor of ~1.2 because of the inverse sixth power relationship. Therefore, the $^{1}H_{PPO}$ intensity observed in this experiment must also originate from PPO that is in relatively close contact with the TFA−titania composite. Also of note is the observation that the maximum $^{19}F\rightarrow{}^{1}H_{PPO}$ signal integration is a factor of 5.7 smaller than the maximum $^{19}F\rightarrow{}^{1}H_{PEO}$ signal integration, although the total PEO proton concentration is about a third of that for PPO. The bulk of this large difference is almost certainly due to only a portion of the PPO in the hybrid being close enough to the TFA−titania to allow efficient magnetization transfer. Weak segregation between the PPO and PEO blocks of the copolymer would result in an interfacial region composed of PEO and PPO both interacting with the TFA−titania. This model explains the above observations and is consistent with ^{1}H $T_{1\rho}$ analysis that revealed significant mobile and rigid PPO components. The rigid PPO component exists within the interfacial region and gives rise to the $^{19}F\rightarrow{}^{1}H$ cross-polarization signal.

Conclusions

The combined results of X-ray scattering, IR/Raman spectroscopy, NMR spectroscopy, and TEM allow for the detailed analysis of both the assembly and the final structure of this new hybrid optical material. The addition of titanium ethoxide to the TFAA solution results in rapid heating, which is evidence of the chemical reaction of the titanium precursor with TFA. IR spectroscopy results suggest that TFA bridges adjacent titanium atoms in a bidentate fashion. SAXS measurements on TFA−titania precursor solution demonstrate that these inorganic units are composed of ~4−5 titanium atoms likely connected by bridging TFA and oxo/hydroxo groups. These stable inorganic clusters are arranged by the surfactant into ordered structures during the first hour following dip-coating when kept in a humid (75% RH) environment via EISA. Raman spectroscopy suggests that this titania has an octahedral, rutile-like local coordination. The stability of this partially cross-linked inorganic network allows for the slow arrangement into highly ordered structures over the course of several days as evidenced by in situ 2D-SAXS. The final material consists of highly ordered domains of inorganic/organic material (Figure 12). The SAXS patterns establish that hybrids with both hexagonal and cubic mesostructures can be synthesized and reveal that the (110) (cubic) or (20) (hexagonal) planes are arranged parallel to the substrate surface. MQ−NMR results demonstrate that the TFA groups are not forming discrete clusters in the material due to fluorophilic interactions, but are instead randomly dispersed. ^{13}C NMR line width and ^{1}H $T_{1\rho}$ relaxation analyses reveal mobile and rigid PPO moieties, whereas the PEO component is predominately rigid. $^{19}F\rightarrow{}^{1}H$ CPMAS and 2D $^{13}C\{^{1}H\}$ measurements show strong spatial proximity between the TFA ligands of the inorganic and the PEO component of the block copolymer. Together, these experiments demonstrate segregation of the PEO within the TFA−titania environment. However, the observation of rigid PPO components in the ^{1}H relaxation data analysis combined with $^{19}F\rightarrow{}^{1}H$ CPMAS buildup curves strongly suggests that the TFA−titania is not completely segregated into the PEO polymer component. All measurements are consistent with the idea that an interphase component exists between the PPO and PEO/inorganic regions composed of inorganic material interacting with the PPO or PPO/PEO mixtures. Such large interfacial regions are common in weakly segregated block copolymer melts, where the degree of incompatibility between the two phases is low.[63]

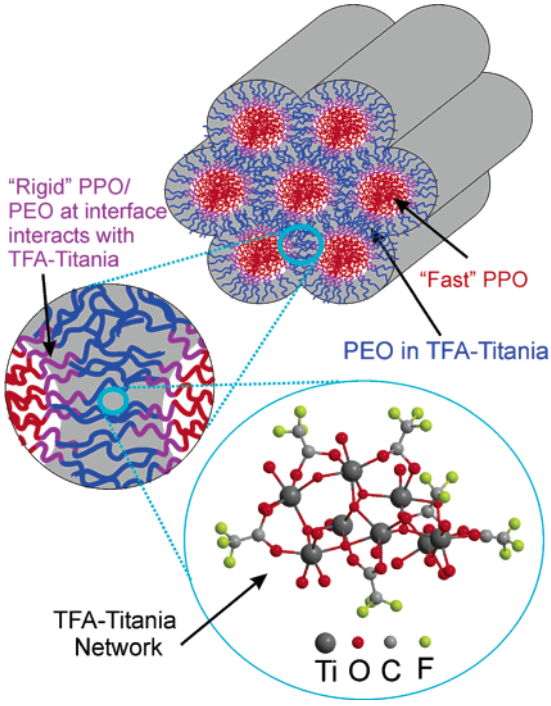

Figure 12. Structural model of titania hybrid showing hexagonal architecture, polymer phase segregation, interfacial region, and representation of the TFA-titania framework.

This detailed understanding of how modified titanium precursors, especially those that change the network-forming behavior and overall hydrophilic character of the titanium, interact with and are arranged in space by the surfactant hydrophilic/hydrophobic domains is an important step in designing new hybrid (inorganic/organic) titania-based optical materials. Especially, such NMR analyses provide insight into microphase separation and interfacial structure in the expansive research field of block copolymer/titania composites. More broadly, the modification of inorganic precursors with strongly binding ligands that prefer the formation of a "glasslike" inorganic component should be quite general and extendable to a variety of other inorganic precursors in order to enhance stability, processability, and optical quality in such new classes of mesostructured hybrids. The compatibility of such modified precursors with block copolymer assembly allows the introduction of a variety of active components within the polymer component of the hybrid material. Concurrently, we now appreciate opportunities to engineer functionality or specific properties into transition metal frameworks by utilizing electronegative complexing ligands. We show that the formation of highly ordered mesostructures is preserved, yet the physical properties of the final materials are significantly altered—in this case, the fluorocarbon modification imparts stability and optical quality to the final hybrid. The presence of chelating/bridging TFA ligands within the titania network suppresses continued condensation of the titania network while still providing the

(63) Khandpur, A. K.; Forster, S.; Bates, F. S.; Hamley, I. W.; Ryan, A. J.; Bras, W.; Almdal, K.; Mortensen, K. *Macromolecules* **1995**, *28*, 8796−8806.

structural stability that allows for the fabrication of optical devices at room temperature.[14] Furthermore, new classes of hybrid materials can now be envisioned—for instance, a discrete, third fluorophilic phase might be fabricated within the inorganic phase by choosing appropriate fluorocarbon-modifying ligands.

Acknowledgment. The authors thank Dr. Youli Li, Dr. Jinping Zhang, Dr. Peter Stoimenov, and Todd Ostomel for their contributions to this work. S.W.B. acknowledges an NSF Graduate Research Fellowship. M.H.B. thanks the Austrian Academy of Sciences for a Max Kade Postdoctoral Fellowship. This work was supported by the NSF (DMR-02-33728), DARPA, and DMEA under the Center for Nanoscience Innovation for Defense (CNID), and made use of MRL Central Facilities supported by the MRSEC Program of the NSF (DMR-00-80034). We thank BASF (Mt. Olive, NJ) for providing Pluronic block copolymers.

Supporting Information Available: ^{19}F MQ−NMR spectra as a function of preparation time and ^{19}F MAS spectra of the hexagonal hybrid material. This material is available free of charge via the Internet at http://pubs.acs.org.

JA050753R